Polyhedron 108 (2016) 36–42

Contents lists available at ScienceDirect

Polyhedron

journal homepage: www.elsevier.com/locate/poly

Extended structure of indium(III) protoporphyrin IX acetate mimics dimer structure of hematin anhydride

Erin L. Dodd, D. Scott Bohle *

Department of Chemistry, McGill University, Montreal, H3A 0B8 Quebec, Canada

ARTICLE INFO

Article history:
Received 2 June 2015
Accepted 29 July 2015
Available online 4 August 2015

Keywords:
Malaria pigment
Protoporphyrin-IX
Indium
Heme stacking
Drug activity

ABSTRACT

A complex of indium(III) protoporphyrin IX acetate was prepared and characterized crystallographically as its pyridine solvate. The structure of the 5-coordinate In complex is dimeric through a strong bridging hydrogen bond between the propionic acid group of one porphyrin unit and the carbonyl of the In-bound acetate, leading to a structure that mimics the reciprocal dimer structure of the malaria pigment hemozoin with an expanded frame. Inter-dimer π-stacking and hydrogen bonding interactions of the propionic acid groups are the dominant structural features. This result, following the report of reciprocal dimers of gallium(III) protoporphyrin IX species, indicates that this is a common motif for metalloprotoporphyrin IX species.

Prevalence of strains of multi-drug resistant malaria is on the rise, with resistance to artesunate therapeutics emerging as a new threat [1] which, combined with wide-spread resistance to quinoline based antimalarials, adds urgency to the search for new therapies. The emergence of a vaccine against *plasmodia* is promising [2], but insufficient to counter the burden of malaria on world health. New strategies, targets, and drugs must be found in the near future [3]. Ambiguities regarding the end target and mode of action of the quinoline and trioxane families of drugs remain [4–7]. Consensus has emerged that the quinoline antimalarials interfere with normal hemoglobin processing in the digestive vacuole of the red blood cell stage of *plasmodia* through disruption of hemozoin formation [6]. The determination that the structure of the native malaria pigment hemozoin is identical to synthetic hematin anhydride (HA or β-hematin) [8,9], confirming prior predictions based on spectroscopy [10–15] and diffraction [16,9,17] for the equivalence of these two materials, has set the stage for the emergence of a chemical model approach to probing the structure of hemozoin and how its solubility and stability may be altered by inducing changes in the solvation, π-stacking, and packing in the crystalline material [18,19].

The substitution of the iron of native heme for the group 13 metal, indium, has been undertaken with the aim of mimicking high-spin iron(III) protoporphyrin IX complexes. Previous work has established that the substitution of gallium(III) for iron provides an extremely useful model for the behavior of iron(III) heme, through both the structural characterization of a gallium(III) protoporphyrin IX dimer and through exploitation of the diamagnetism of the gallium metal to probe the solution dynamics of these complexes, in particular the reactivity at the propionic acid groups, through NMR and fluorescence [20,21]. The d^{10} gallium model, however, undergoes facile ligand exchange and readily forms a 6-coordinate complex which is the first step towards substituting the opposite axial ligand. Crystal field and spin imposed barriers for these types of substitution reactions slow the corresponding reactions for high-spin iron(III). Though isoelectronic with its group 13 congener, indium(III) is larger with an ionic radius of 0.94 Å [22]. The metal atom of an indium(III) complex of protoporphyrin IX would therefore be forced out of the plane of the porphyrin, largely precluding a 6 co-ordinate species.

The acetate complex of indium(III) protoporphyrin IX, **1**, was found to crystallize in an apparent expansion of the reciprocal dimer motif, with the 'bridging' propionic acid group hydrogen-bonded to the bound acetate ligand and the orientation of the chiral porphyrin ligands unambiguously determined to be centrosymmetric across an inversion center at the center of the dimer. These structural features bear a strong similarity to the structure of hematin anhydride itself. In addition to this new motif, this is the first report of a single crystal structure of an indium(III) protoporphyrin IX complex.

The intra-'dimer' porphyrin-porphyrin π-stacking interactions deviate slightly from those of hematin anhydride, with a greater intra-dimer porphyrin offset observed in hematin anhydride than we see in the indium analog. These porphyrin offset distances will be shown to be of minimal relevance to the overall stability and

* Corresponding author. Tel.: +1 514 398 7409; fax: +1 514 398 3797.
E-mail address: scott.bohle@mcgill.ca (D.S. Bohle).

http://dx.doi.org/10.1016/j.poly.2015.07.072
0277-5387/

solubility of the crystals through comparison to two crystallographically isostructural forms of gallium(III) octaethylporphyrin methoxide, one of which is novel.

1. Materials and methods

All porphyrins were purchased from Frontier Scientific, Inc. Indium chloride hydrate and gallium chloride were purchased from STREM chemicals. All other reagents were purchased from Sigma–Aldrich and used without further purification. HPLC-grade methanol, HPLC-grade dichloromethane, and double-distilled 2,6-lutidine were purchased from Sigma–Aldrich and used without further purification. NMR-grade d_4-methanol was purchased from Cambridge Isotopes and used without further purification. All ^{1}H NMR experiments were performed on a 500 MHz Varian Mercury NMR spectrometer and analyzed using MestreNOVA software. UV–Vis spectroscopy was performed on a Hewlett Packard 845× series UV–Vis ChemStation (Agilent). Infrared spectroscopy was performed on an ABB Bomem MB series IR spectrometer. Elemental analysis was performed at the University of Montreal.

A diagram of the porphyrin numbering scheme is included in the Supplementary section.

1.1. Preparation of indium(III) protoporphyrin IX chloride, In(PPIX)Cl (**2**)

Protoporphyrin IX dimethyl ester (2.5 mmol) was suspended in 2,6-lutidine (20 mL). Indium trichloride hydrate (6 mmol) was added to the protoporphyrin IX dimethyl ester under a stream of nitrogen. 2,6-Lutidine was added to increase the volume to 20 mL. The reaction mixture was heated at 150 °C for 1.5 h, then cooled, diluted with 500 mL concentrated brine, then acidified to pH = 4 with 20% aqueous citric acid. The pink precipitate was collected by filtration and washed with distilled water (3 × 100 mL). The solid collected was dissolved in methanol (200 mL) and washed though the frit. The solvent was evaporated and the solid was dried *in vacuo* to yield purple-red solid in 95% yield. UV–Vis λ_{max} (MeOH): A_{max} [nm] (ε(Lmol^{-1} cm^{-1})): 407 (277 000), 542 (18,300), 580 (18,000). IR (KBr) (cm^{-1}): 1732 and 1622 ($\nu(CO_2)_{sym}$), 1438 ($\nu(CO_2)_{asym}$) ^{1}H NMR: (very dilute 3 * 10^{-8} M in d_4-methanol, referenced to TMS), 500 MHz) δ(*ppm*): 3.32 (propionic acid side group $H_{2\beta}$ and $H_{18\beta}$, 4H, b), 3.80 (methyl $H_{3\alpha}$, 3H, s), 3.83 (methyl $H_{17\alpha}$, 3H, s), 3.88 (methyl $H_{8\alpha}$, 3H, s), 3.91 (methyl $H_{12\alpha}$, 3H, s), 4.58 (propionic acid $H_{2\alpha}$ and $_{18\alpha}$, 4H, b), 6.35 (vinyl $H_{7\beta}$ trans to porphyrin, 1H, d, $^3J_{7\alpha\text{-}7\beta(trans)}$ = 11.5 Hz), 6.36 (vinyl $H_{12\beta}$ trans to porphyrin,1H, d, $^3J_{12\alpha\text{-}12\beta(trans)}$ = 11.5 Hz), 6.56 (vinyl $H_{7\beta}$ cis to porphyrin, 1H, $^3J_{7\alpha\text{-}7\beta(cis)}$=17.8 Hz), 6.58 (vinyl $H_{12\beta}$ cis to porphyrin, 1H, $^3J_{12\alpha\text{-}12\beta(cis)}$ = 17.8 Hz), 8.54 (vinyl $H_{7\alpha}$, 1H, dd, $^3J_{7\alpha\text{-}7\beta(cis)}$ = 17.8 Hz, $^3J_{7\alpha\text{-}7\beta(trans)}$ = 11.5 Hz), 8.56 (vinyl $H_{12\alpha}$, 1H, dd, $^3J_{12\alpha\text{-}12\beta(cis)}$ = 17.8 Hz, $^3J_{12\alpha\text{-}12\beta(trans)}$ = 11.5 Hz), 10.65 (methine H_{15}, 1H, s), 10.67 (methine H_5, 1H, s), 10.73 (methine H_{20}, 1H, b), 10.77 (methine H_{10}, 1H, s).

1.2. Preparation of indium(III) protoporphyrin IX hydroxide, In(PPIX)(OH) (**3**)

indium(III) protoporphyrin IX chloride (1 mmol) was dissolved in methanol (50 mL). KOH in methanol (100 mL, 2.2 M) was added to this solution which was stirred for 1 h at room temperature, then acidified to pH = 4 with 20% aqueous citric acid, diluted to over 600 mL with concentrated brine and filtered. The solid collected was re-dissolved in methanol (75 mL) and washed though the frit. Dark purple In(PPIX)(OH) is obtained upon evaporation of solvent and dried *in vacuo*. Yield was 85%. UV–Vis λ_{max} (MeOH): A_{max} [nm] (ε(Lmol^{-1} cm^{-1})): 407 (329,000), 542 (20,600), 580 (20,400). IR (KBr) (cm^{-1}): 1725 and 1624 ($\nu(CO_2)_{sym}$), 1386 ($\nu(CO_2)_{asym}$) ^{1}H NMR: (0.18 M in d_4-methanol, referenced to TMS), 500 MHz) δ(*ppm*): 3.22 (propionic acid $H_{2\beta}$ and $H_{18\beta}$, 4H, b), 3.76 (methyl $H_{3\alpha}$, 3H, s), 3.79 (methyl $H_{17\alpha}$, 3H, s), 3.87 (methyl $H_{8\alpha}$, 3H, s), 3.89 (methyl $H_{12\alpha}$, 3H, s), 4.59 (propionic acid $H_{2\alpha}$ and $_{18\alpha}$, 4H, t, ^3J = 7.3), 4.60 (propionic acid $H_{2\alpha}$ and $_{18\alpha}$, 4H, t, ^3J = 7.3), 6.36 (vinyl $H_{7\beta}$ trans to porphyrin, 1H, d, $^3J_{7\alpha\text{-}7\beta(trans)}$ = 11.5 Hz), 6.37 (vinyl $H_{12\beta}$ trans to porphyrin,1H, d, $^3J_{12\alpha\text{-}12\beta(trans)}$ = 11.5 Hz), 6.57 (vinyl $H_{7\beta}$ cis to porphyrin, 1H, $^3J_{7\alpha\text{-}7\beta(cis)}$ = 17.6 Hz), 6.58 (vinyl $H_{12\beta}$ cis to porphyrin, 1H, $^3J_{12\alpha\text{-}12\beta(cis)}$ = 17.9 Hz), 8.54 (vinyl $H_{7\alpha}$, 1H, dd, $^3J_{7\alpha\text{-}7\beta(cis)}$ = 17.6 Hz, $^3J_{7\alpha\text{-}7\beta(trans)}$ = 11.5 Hz), 8.56 (vinyl $H_{12\alpha}$, 1H, dd, $^3J_{12\alpha\text{-}12\beta(cis)}$ = 17.6 Hz, $^3J_{12\alpha\text{-}12\beta(trans)}$ = 11.5 Hz), 10.66 (methine H_{15}, 1H, s), 10.68 (methine H_5, 1H, s), 10.74 (methine H_{20}, 1H, b), 10.69 (methine H_{10}, 1H, s).

1.3. Preparation of In(PPIX)(OAc)·py (**1**)

10 mg of In(PPIX)Cl was dissolved in a mixture of acetic acid (glacial, 1 mL) and pyridine (2 mL). Crystals were allowed to form with slow evaporation in constant atmosphere.

1.4. Preparation of Ga(OEP)Cl (**4**)

Octaethylporphine (0.47 mmol) was suspended in 2,6-lutidine (10 mL). In a glove bag assembly under nitrogen, gallium trichloride (17 mmol) was dissolved in 2,6-lutidine (10 mL) under nitrogen atmosphere, and added dropwise to the porphyrin under a stream of nitrogen. The reaction mixture was refluxed at 150 °C for 1.5 h then cooled, diluted with 500 mL distilled water and filtered, washing with distilled water. The dry solid collected was re-dissolved in 75 mL dichloromethane and washed though the frit. Ga(OEP)Cl is obtained upon immediate evaporation of solvent at room temperature *in vacuo*. ^{1}H NMR: (0.18 M in d_4-methanol, referenced to TMS), 500 MHz) δ(*ppm*): 1.84 (CH_3, 24H, t, J^3 = 7.62 Hz), 3.92 (CH_2, 16H, quar, J^3 = 7.62 Hz), 9.87 (CH, 4H, s). Elemental analysis: found (expected) C, 67.48 (67.78); H, 7.40 (6.95); N, 8.55 (8.78). Spectroscopically identical to literature report [23].

1.5. Preparation of Ga(OEP)(OH) (**5**)

Gallium(III) octaethylporphyrin chloride (0.47 mmol) was dissolved in methanol (50 mL). KOH in methanol (100 mL, 2.2 M) was added to this solution which was stirred for 1 h at room temperature, then acidified to pH = 4 with 20% aqueous citric acid, diluted to over 600 mL with distilled water and filtered. The dry solid collected was re-dissolved in 75 mL dichloromethane and washed though the frit. Ga(OEP)(OH) is obtained upon evaporation of solvent. ^{1}H NMR: (0.18 M in d_4-methanol), 500 MHz) δ(*ppm*): 1.82 (CH_3, 24H, t, J^3 = 7.67 Hz), 3.88 (CH_2, 16H, quar, J^3 = 7.67 Hz), 9.80 (CH, 4H, s). Elemental analysis: found: C, 70.03; H, 7.56; N, 8.78; expected if Ga(OEP)(OH): C, 69.80; H, 7.32; N, 9.04; expected if Ga(OEP)(OH)(H_2O): C, 67.82; H, 7.43; N, 8.79. Spectroscopically identical to literature report [24].

1.6. Preparation of Ga(OEP)(OMe) (slow growth) (**6a**)

Gallium(III) octaethylporphyrin chloride (500 mg) was dissolved in methanol (100 mL) and left sitting for two weeks undisturbed and dark. Large pink trapezoidal crystals were harvested for crystallographic study. Spectroscopically identical to literature report [24].

1.7. Preparation of Ga(OEP)(OMe)·3MeOH (fast growth) (**6b**)

Gallium(III) octaethylporphyrin chloride (500 mg) was dissolved in methanol (100 mL). Addition of a base (acetate,

triethylamine, or potassium hydroxide in methanol) afforded large pink trapezoidal crystals in less than an hour, which were harvested for crystallographic study. Alternative preparation: gallium(III) octaethylporphyrin hydroxide was dissolved in methanol and left sitting for an hour. Large pink trapezoidal crystals were harvested for crystallographic study.

2. Results and discussion

Like the syntheses of the iron analogs, In(PPIX)(OAc) crystals were obtained by a slow crystallization in an anhydrous solvent mixture. In each case, a base (2,6-lutidine or pyridine) is used as bases to promote carboxylate ligation. In the iron species, DMSO aids in solubility of the heme species and slows the crystallization by competitively binding to iron. Use of acetic acid in the indium preparation provided the acetate ligand of the product. The ratio of acetic acid to pyridine was 1:2, ensuring that the environment was overall basic in order to drive chelation. Similar approaches to attempt to crystallize the $(In(PPIX))_2$ dimer, an analog of HA, in the absence of an external carboxylate source were unsuccessful and lead to a mixture of amorphous solid products as determined by IR.

Scheme 1 outlines the preparations of hematin anhydride [9], the diethyl analog mesohematin anhydride [19], and solvated crystalline In(PPIX)(OAc). The preparation of these compounds does not necessarily predict the solvation, which is likely driven by differences in the crystalline packing that disfavor other potential hydrogen bonding pairings.

Crystallization of indium(III) protoporphyrin IX acetate (In(PPIX)(OAc)) in pyridine/acetic acid yielded crystals of the molecule as a pyridine solvate which were suitable for X-ray diffraction. Although the porphyrin units are monomeric, hydrogen bonding in the crystalline solid gives a structure that is pseudo-HA dimeric in

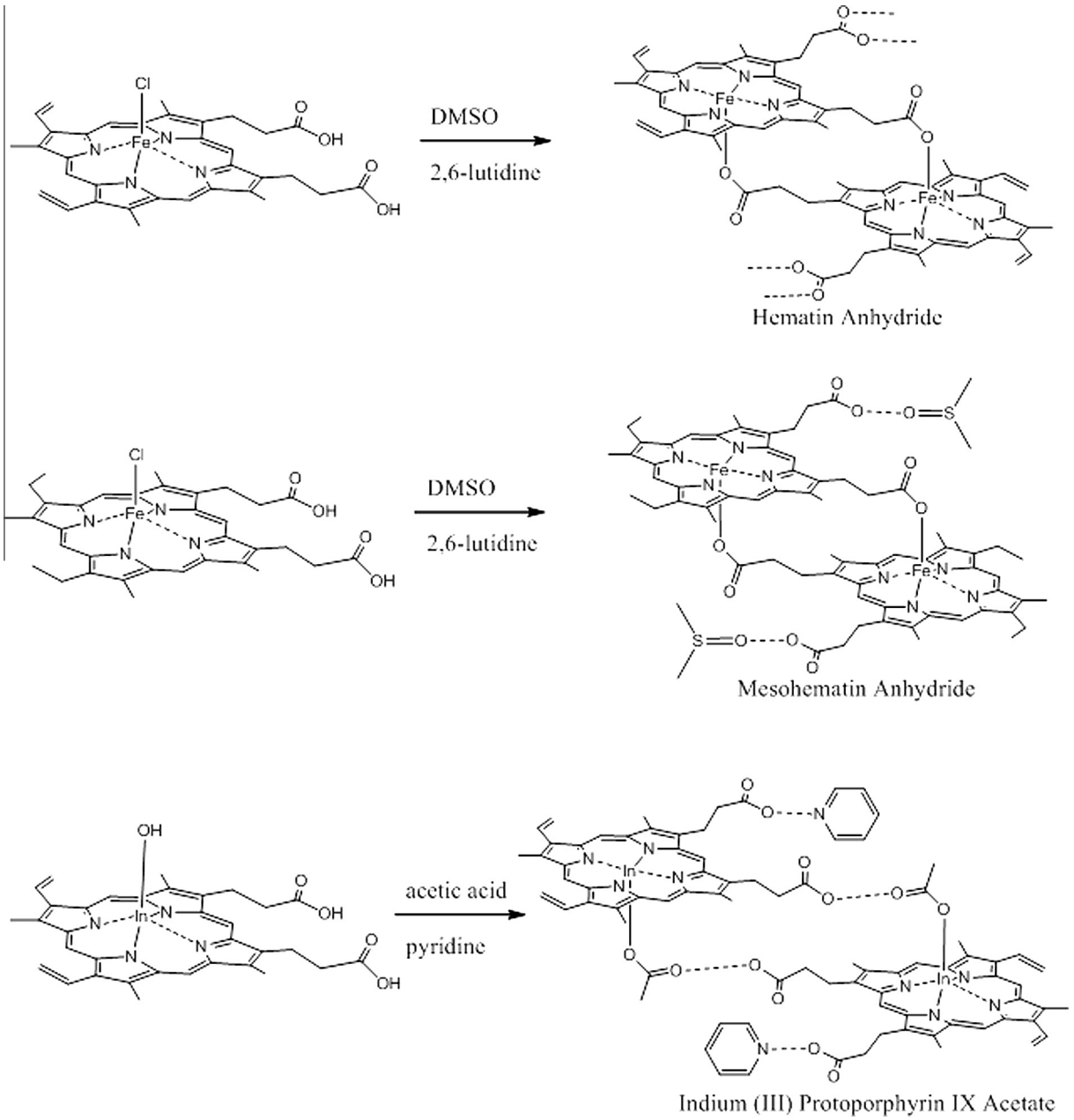

Scheme 1. Crystallographic data for metalloporphyrins.

nature with a hydrogen bond between propionic acid O(1) and the acetate O(5) at 2.623 Å connecting two monomeric metalloporphyrin units, as well as another hydrogen bond between the second propionic acid O(3) and the solvated pyridine N(5) at 2.618 Å. The hydrogen bond has a significant effect on the nature of the C–O bonds of the acetate ligand in which the C-O bond lengths are nearly equivalent at 1.266(7) and 1.237(8). This is comparable to acetate C–O bond length ratios observed in another known monohapto indium porphyrin structure, acetato-[meso-tetra(p-chlorophenyl)porphyrinato]indium(III) [25].

A surprising and significant similarity between the structure of **1** and the hematin anhydride analog, mesohematin anhydride, is the presence of a pyridine solvate that mimics the position of the dimethylsulfoxide solvate of that complex, which forms a hydrogen bond to the free propionic acid sidechain. This pyridine solvate is bound by a hydrogen bond at an O–N separation 2.618 Å compared to O–O 2.598(8) Å in mesohematin anhydride and 2.830(7) Å in hematin anhydride. The pyridine solvate molecules of **1** contribute to the crystal packing arising from the free propionic acid side chain, filling the gap in the expanded space between the porphyrins (Table 1).

It is notable that the position of vinyl and methyl groups on the porphyrin periphery was well ordered, suggesting no significant disorder in the orientation of the porphyrin units. Attempts have been made to ascribe the mosaicity and disorder in the structure of microcrystalline hemozoin derived from parasite and observed

Table 1
Sample and crystal data.

	In(PPIX)(OAc)·py	Ga(OEP)(OMe)	Ga(OEP)(OMe)·3MeOH
Chemical formula	$C_{41}H_{40}InN_5O_6$	$C_{37}H_{51}GaN_4O$	$C_{40}H_{59}GaN_4O_4$
Formula weight	813.6	637.54	729.63
T (K)	100(2)	295(2)	296(2)
λ (Å)	0.71073	0.71073	0.71073
Crystal system	triclinic	monoclinic	monoclinic
Space group	$P\bar{1}$	$P2(1)/c$	$P2(1)/n$
Unit cell dimensions			
a (Å)	10.1093(8)	13.3442(10)	15.1155(18)
b (Å)	12.9757(10)	13.6892(10)	14.0004(16)
c (Å)	14.7210(11)	18.9551(14)	18.881(2)
α (°)	96.6280(10)	90	90
β (°)	103.3870(10)	106.3760(10)	98.0490(10)
γ (°)	100.1180(10)	90	90
V (Å^3)	1824.6(2)	3322.1(4)	3956.3(8)
Z	2	4	4
D_{calc} (Mg/cm^3)	1.481	1.275	1.225
Absorption coefficient (mm^{-1})	0.704	0.863	0.739
F(000)	836	1360	1560
Crystal size (mm)	0.01 × 0.02 × 0.30	0.50 × 0.50 × 0.80	0.05 × 0.30 × 0.50
θ range for data collection (°)	1.44–25.03	2.18–28.19	1.62–28.41
Index ranges	$-12 \leqslant h \leqslant 12$, $-15 \leqslant k \leqslant 15$, $-17 \leqslant l \leqslant 17$	$-17 \leqslant h \leqslant 17$, $-18 \leqslant k \leqslant 18$, $-24 \leqslant l \leqslant 24$	$-19 \leqslant h \leqslant 20$, $-18 \leqslant k \leqslant 18$, $-25 \leqslant l \leqslant 24$
Reflections collected	17318	35282	44471
Independent reflections (R_{int})	6372 (0.0321)	7591 (0.0468)	9302 (0.0268)
Coverage of independent reflections (%)	98.90	92.80	93.50
Absorption correction	multi-scan	none	multi-scan
Max. and min. transmission	0.9930 and 0.8167	not corrected	0.9640 and 0.7090
Refinement method	Full-matrix least-squares on F^2	Full-matrix least-squares on F^2	Full-matrix least-squares on F^2
Data/restraints/parameters	6372/0/486	7591/0/397	9302/0/457
Goodness-of-fit (GOF) on F^2	1.093	1.128	1.045
Final R indices [$I > 2\sigma(I)$]	$R_1 = 0.0503$, $wR_2 = 0.1180$	$R_1 = 0.0389$, $wR_2 = 0.0796$	$R_1 = 0.0264$, $wR_2 = 0.0693$
R indices (all data)	$R_1 = 0.0589$, $wR_2 = 0.1222$	$R_1 = 0.0590$, $wR_2 = 0.0919$	$R_1 = 0.0329$, $wR_2 = 0.0720$
Largest diff. peak and hole (e Å^{-3})	2.300 and −1.395	0.715 and −0.616	0.382 and −0.294

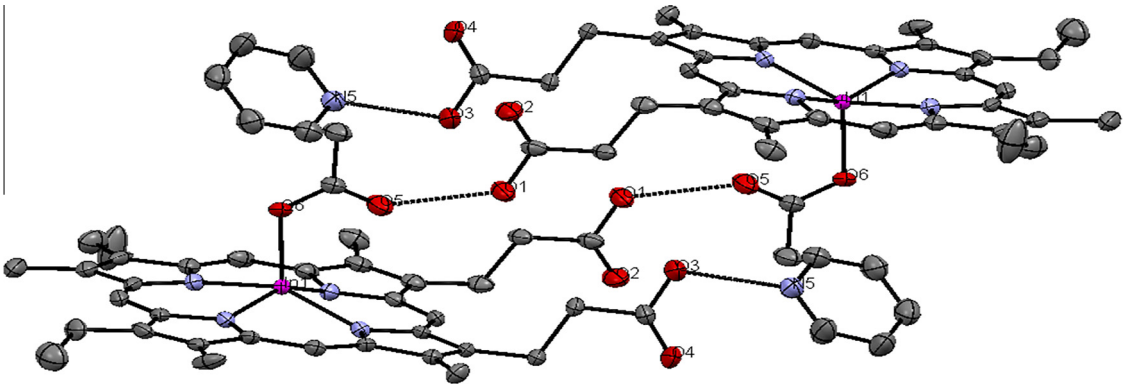

Fig. 1. ORTEP diagram of In(PPIX)(OAc)·py, **1**, with 40% thermal ellipsoids showing only slight disorder in the vinyl groups. Carbon-bound hydrogens are omitted for clarity. Key metric parameters (Å) include: In–O(6) 2.128(4), In–N(1) 2.133(5), In–N(2) 2.139(5), In–N(3) 2.150(5), In–N(4) 2.120(5), O(6)–C(35) 1.266(7), O(5)–C(35) 1.237(8), O(1)–C(23) 1.322(7), O(2)–C(23) 1.201(7), O(3)–C(34) 1.303(8), O(4)–C(34) 1.212(8).

extra peaks in the powder X-ray diffraction pattern of synthetic hematin anhydride to isomerism in the enantiofacial symmetry of the porphyrin, the monomeric units of which are chiral when metallated [26]. The observed order in the In(PPIX)(OAc) structure, as well as in the Ga(PPIX) species reported previously [21,27], present a strong argument for the ability of the porphyrin units to differentiate between the methyl and vinyl groups on their periphery in their crystal packing during slow growth. The disorder observed in the powder diffraction data for the high-quality microcrystalline iron species may therefore stem more from bulk properties than isomerism within each crystal (Fig. 1).

Discussion concerning the relationship between crystal packing in hemozoin and its stability/insolubility has recently been dominated by the suggestion that the role of π-stacking between porphyrin units is important. Scheidt and Lee have devised a useful set of structural criteria for determining the degree of p-interac-

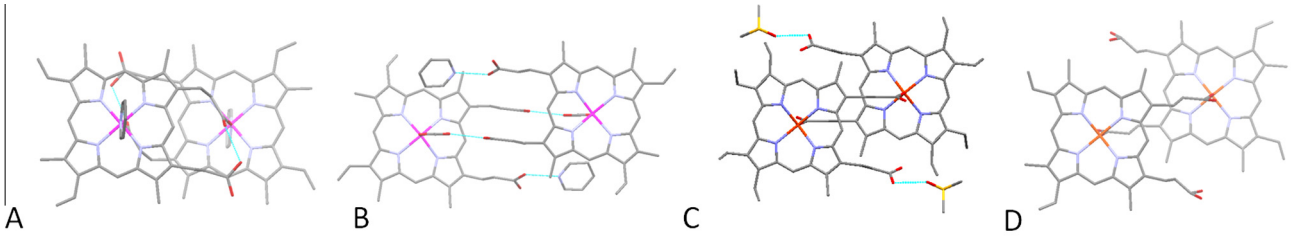

Intra-dimer parameters	**A** $[Ga(PPIX)(py)]_2$	**B** In(PPIX)(OAc) 2(py)	**C** $[Fe(MPIX)]_2$ 2(DMSO)	**D** $[Fe(PPIX)]_2$
M-O distance	2.010 (2)	2.128(4)	1.905(7)	1.886(2)
M out of plane	0.031	0.526	0.486	0.47
M-M distance	8.199	13.128	9.13	9.047
mean porphyrin plane separation	4.651	6.030	4.704	4.724

Fig. 2. Contrast in intra-dimer and inter-dimer porphyrin overlap between gallium, indium, and iron dimers (a) $[Ga(PPIX)(py)]_2$; (b) the 'expanded' hydrogen bond dimer of In(PPIX)(OAc)·py; (c) DMSO-solvated mesohematin anhydride; (d) hematin anhydride.

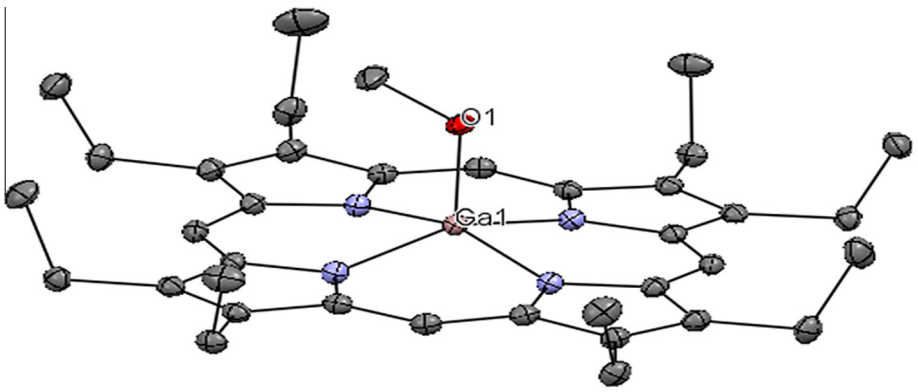

Fig. 3. ORTEP diagram of Ga(OEP)(OMe) in *P*2(1)/*c*, thermal ellipsoids at 40%. Carbon-bound hydrogens are omitted for clarity. Key metric parameters (Å) include: Ga(1)–O(1) 1.8304(17), Ga(1)–N(1) 2.0465(18), Ga(1)–N(2) 2.0366(18) Ga(1)–N(3) 2.0464(17) Ga(1)–N(4) 2.0513(17). This structure is included in the CCDC as CCDC #858900.

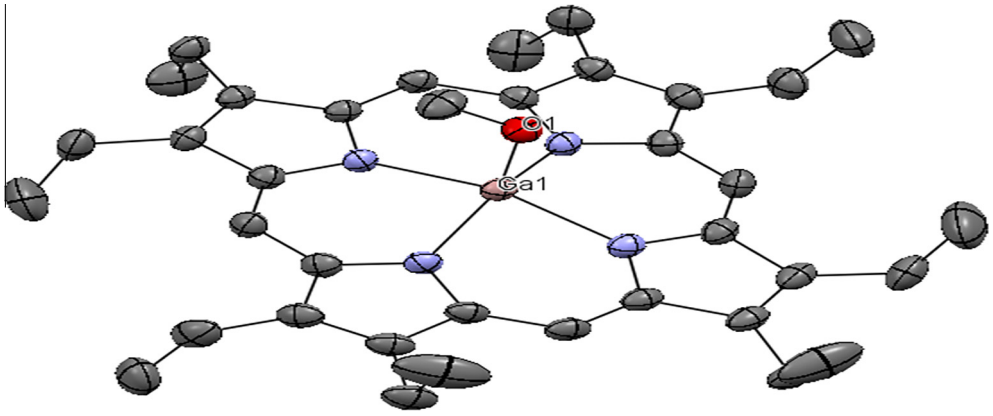

Fig. 4. ORTEP diagram of **6b**, Ga(OEP)(OMe) in *P*2(1)/*n*, thermal ellipsoids at 40%. Carbon-bound hydrogens are omitted for clarity. Key metric parameters (Å) include: Ga(1)–O(1) 1.8650(9), Ga(1)–N(1) 2.0326(11), Ga(1)–N(2) 2.0325(11) Ga(1)–N(3)2.0415(11), Ga(1)–N(4) 2.0477(11). Solvate is methanol.

tions in porphyrins in terms of the separation of the metals, the mean-plane separation, and the lateral shift or offset [28]. The expanded porphyrin pseudo-HA dimer motif provides an opportunity to probe this further in comparison to the known iron analogs, and therefore we have amassed the parameters which result from Scheidt's analysis of π-stacking for each of the species in Fig. 2. The noted absence of any overlap at all between intra-dimer porphyrin rings ensures that any π-stacking considered must be inter-dimer, and the values observed indicate weak π-stacking between the adjacent outer faces of the dimers. Yet, **1** is sparingly soluble in most solvents much as mesohematin anhydride is [19].

While the intra-'dimer' porphyrin separation is very large, with a mean plane separation of 6.030 Å, the inter-'dimer' porphyrin – porphyrin separation between In(PPIX)(OAc) molecules is small at 3.447 Å, and the overlap is considerable with an offset of only 0.13 Å (Fig. S4). In the overall packed structure of these crystals (Figs. S2–S4), it can be concluded that the degree of overlap corresponds with a strength of porphyrin π–π stacking that is far higher than that observed in hematin anhydride itself. This adds to the stability of the solid crystalline form, and thus we observe low solubility of these crystals in any solvent.

To extend this analysis, we considered two distinct crystal morphologies of gallium(III) octaethylporphyrin methoxide, which differ in their crystal packing. Ga(OEP)Cl exchanges ligand Cl^- slowly over time with methanol upon dissolution of the solid to yield the methoxy adduct, as determined unambiguously by X-ray crystallography of the solid which crystallizes upon concentration (Figs. 3 and 4). No change in chemical environment is determined by either NMR or UV analysis of Ga(OEP)X in methanol solution, thus we conclude that the exchange dynamics lead to an average spectrum that does not change appreciably. Crystals of Ga(OEP)(OMe) grow spontaneously in solutions of Ga(OEP)X in methanol, and form much faster from Ga(OEP)(OH), or from Ga(OEP)Cl in the presence of any strong base. In short, the ligand exchange is rapid and favors the 'hardest', most basic anionic ligand. Porphyrin stacking and side chain orientations have been found to be comparable to those in known gallium porphyrin structures [29–31]. No change in chemical environment is determined by either NMR or UV analysis of Ga(OEP)(X) in methanol solution, thus we conclude that the exchange dynamics lead to an average spectrum that does not change appreciably. Crystals of Ga(OEP)(OMe) grow spontaneously in solutions of Ga(OEP)X in methanol upon concentration, and form much faster in the presence of any strong base to initiate deprotonation of the methanol solvent.

Ga(OEP)(OMe) crystallizes in two different settings, both monoclinic. The porphyrin stacking and ethyl side chain orientations of each have been found to be comparable to those in known gallium porphyrin structures [29–31] with the metal 0.49 Å out of the plane of the porphyrin and very minor ruffling in the porphyrin itself in either structure. In the first structure **6a**, the ethyl side-chains orient in a half-up, half-down arrangement that allows for packing with pairs of porphyrins π-stacked with planes overlapping imperfectly at a separation of 3.532 Å and metal–metal distance of 5.713 Å. The porphyrin offset is just enough to perfectly overlap metals with the centre of a pyrrole ring of the other porphyrin of the pair in the manner discussed by Abraham et al. [32] In the second *P*2(1)/*n* structure **6b**, the porphyrins also form face-to-face pairs. The porphyrinpairs experience slightly less offset, with a smaller plane separation of 3.365 Å and metal–metal distance of 4.468 Å, and a gallium atom located closer to the porphyrin plane at 0.40 Å. This indicates higher π-stacking between the porphyrin units. These crystals are less dense, with large spaces for solvated methanol molecules which are connected through hydrogen bonding in a chain from the gallium-bound methoxide ligand in a half-hexagon motif. Each crystal stacks in a herringbone arrangement of face-to-face pairs (Figs. S5 and S6).

Addition of one equivalent of acetic acid immediately following dissolution of Ga(OEP)(OH) prevents this rapid reaction with solvent and consequent precipitation, giving a stable pink solution in methanol, and causes crystals of **6b**, once formed, to re-dissolve.

The herringbone arrangement of both Ga(OEP)(OMe) structures is distinct from the parallel orientation of the porphyrin planes in all the natural porphyrin species, which is likely favored by the additional orienting force of the hydrogen bonding attractions of the propionates. Thus any direct comparison of solubility is of little worth. However, the differences conferred by the slight differences in π-overlap and solvation are significant, with a higher degree of overlap in the second structure leading to a large reduction in solubility.

3. Conclusions

In conclusion, we have prepared an indium(III) analog of heme which crystallizes in a motif that mimics the reciprocal dimer structure of hematin anhydride. The addition of the structure of the In(PPIX)(OAc) pseudo-HA dimer to the already growing family of structures of metalloprotoporphyrin reciprocal dimers strongly suggests that this structural motif is a thermodynamically favored one for natural porphyrins, driven by the hydrogen-bonding capabilities of the propionate side chains of the porphyrin. It is noteworthy that many preparations of hematin anhydride employ either acetic or propionic acids. Either acid may form an iron complex analogous to **1** and this could contribute to the generally high mosaicity found in the products of these preparations. Considerable caution needs to be used when interpreting the nature of the London forces behind the dimer/dimer interactions in the crystalline phase, and the diversity observed across the compound series presented here makes clarifies the dependence of the variation on the other factors involved in the crystalline packing for each species. This is an important consideration in analyses of both the growth of hemozoin crystals within a malaria parasite, and in the mode of action of putatively crystallization inhibiting drugs such as the quinoline antimalarials which is often discussed using docking models to the known dimer structure. The disruption of that structure by solvates as observed in the indium(III) protoporphyrin IX acetate and mesohematin anhydride structures indicates that disruption of the hydrogen bonding network of the hemozoin must be taken into account in any study of the binding of drug to heme species, as indeed has been seen to be the case in the reported reciprocal dimer of gallium (III) protoporphyrin IX bound to two chloroquine molecules [27].

Acknowledgements

We gratefully acknowledge support from NSERC and the CRC for this research.

Appendix A. Supplementary data

CCDC 1404010, 1404139, and 1404040 contains the supplementary crystallographic data for this paper. These data can be obtained free of charge via http://www.ccdc.cam.ac.uk/conts/retrieving.html, or from the Cambridge Crystallographic Data Centre, 12 Union Road, Cambridge CB2 1EZ, UK; fax: (+44) 1223 336 033; or e-mail: deposit@ccdc.cam.ac.uk. Supplementary data associated with this article can be found, in the online version, at http://dx.doi.org/10.1016/j.poly.2015.07.072.

References

[1] M. Enserink, Science 328 (2010) 844.
[2] G. Vogel, Science 328 (2010) 847.

[3] M. Enserink, Science 328 (2010) 846.
[4] L.-W. Cui, X.-Z. Su, Expert Rev. Anti-Infective Ther. 7 (2009) 999.
[5] J. Wang, L. Huang, J. Li, Q. Fan, Y. Long, Y. Li, B. Zhou, PLoS One 5 (2010).
[6] T.J. Egan, Trends Parasitol. 22 (2006) 235.
[7] J. Lelievre, A. Berry, F. Benoit-Vical, Curr. Opin. Invest. Drugs 8 (2007) 117.
[8] N. Klonis, R. Dilanian, E. Hanssen, C. Darmanin, V. Streltsov, S. Deed, H. Quiney, L. Tilley, Biochemistry 49 (2010) 6804.
[9] S. Pagola, P.W. Stephens, D.S. Bohle, A.D. Kosar, S.K. Madsen, Nature 404 (2000) 307.
[10] A.F.G. Slater, W.J. Swiggard, B.R. Orton, W.D. Flitter, D.E. Goldberg, A. Cerami, G.B. Henderson, Proc. Natl. Acad. Sci., U.S.A 88 (1991) 325.
[11] D.S. Bohle, B.J. Conklin, D. Cox, S.K. Madsen, S. Paulson, P.W. Stephens, G.T. Yee, ACS Symp. Ser. 572 (1994) 497.
[12] D.S. Bohle, P. Debrunner, P.A. Jordan, S.K. Madsen, C.E. Schulz, J. Am. Chem. Soc. 120 (1998) 8255.
[13] A. Sienkiewicz, J. Krzystek, B. Vileno, G. Chatain, A.J. Kosar, D.S. Bohle, L. Forro, J. Am. Chem. Soc. 128 (2006) 4534.
[14] B.R. Wood, D. McNaughton, Expert Rev. Proteom. 3 (2006) 525.
[15] M.-J. Bellemare, D.S. Bohle, C.-N. Brosseau, E. Georges, M. Godbout, J. Kelly, M.L. Leimanis, R. Leonelli, M. Olivier, M. Smilkstein, J. Phys. Chem. B 113 (2009) 8391.
[16] D.S. Bohle, R.E. Dinnebier, S.K. Madsen, P.W. Stephens, J. Biol. Chem. 272 (1997) 713.
[17] D.S. Bohle, A.D. Kosar, P.W. Stephens, Acta Crystallogr., Sect. D, Biol. Crystallogr. D58 (2002) 1752.
[18] D.S. Bohle, E.L. Dodd, P.W. Stephens, Chem. Biodivers. 2012 (1891) 9.
[19] D.S. Bohle, E.L. Dodd, A.J. Kosar, L. Sharma, P.W. Stephens, L. Suárez, D. Tazoo, Angew. Chem. Int. 50 (2011) 6151.
[20] D.S. Bohle, E.L. Dodd, T.B.J. Pinter, M.J. Stillman, Inorg. Chem. (2012).
[21] D.S. Bohle, E.L. Dodd, Inorg. Chem. 51 (2012) 4411.
[22] R.D. Shannon, Acta Crystallogr. Sect. A A32 (1976) 751.
[23] K.M. Kadish, B. Boisselier-Cocolios, A. Coutsolelos, P. Mitaine, R. Guilard, Inorg. Chem. 24 (1985) 4521.
[24] K.M. Kadish, J.L. Cornillon, A. Coutsolelos, R. Guilard, Inorg. Chem. 26 (1987) 4167.
[25] Y.-Y. Lee, J.-H. Chen, H.-Y. Hsieh, Polyhedron 22 (2003) 1633.
[26] T. Straasø, S. Kapishnikov, K. Kato, M. Takata, J. Als-Nielsen, L. Leiserowitz, Cryst. Growth Des. 11 (2011) 3342.
[27] E.L. Dodd, D.S. Bohle, Chem. Commun. 50 (2014) 13765.
[28] W.R. Scheidt, Y.J. Lee, Struct. Bonding (Berlin) 64 (1987) 1.
[29] A. Coutsolelos, R. Guilard, D. Bayeul, C. Lecomte, Polyhedron 5 (1986) 1157.
[30] A.G. DiPasquale, J.M. Mayer, J. Am. Chem. Soc. 2008 (1812) 130.
[31] Y.-Y. Hsieh, Y.-H. Sheu, I.C. Liu, C.-C. Lin, J.-H. Chen, S.-S. Wang, H.-J. Lin, J. Chem. Crystallogr. 26 (1996) 203.
[32] P. Leighton, J.A. Cowan, R.J. Abraham, J.K.M. Sanders, J. Org. Chem. 53 (1988) 733.